Supporting Information to

CO_2-free electric power circulation via direct charge and discharge using the glycolic acid/oxalic acid redox couple

R. Watanabe,[ab] M. Yamauchi,*[ab] M. Sadakiyo,[ab] R. Abe[bc] and T. Takeguchi[bd]

[a] International Institute for Carbon Neutral Energy Research (WPI-I^{2}CNER), Kyushu University, Motooka 744, Nishi-ku, Fukuoka 819-0395, Japan.
[b] CREST, JST, 4-1-8 Honcho, Kawaguchi, Saitama 332-0012, Japan.
[c] Graduate School of Engineering, Kyoto University, Katsura, Nishikyo-ku, Kyoto 615-8510, Japan.
[d] Department of Chemistry and Bioengineering, Faculty of Engineering, Iwate University, 4-3-5 Ueda, Morioka, Iwate 020-8551, Japan.

METHODS

Materials

Titanium tetrabutoxide (95.0%), 2-propanol (99.9%), sodium sulfate (99.0%), methanol (99.5%), sulfuric acid (95.0%), oxalic acid (**OX**, 98.0%), glyoxylic acid monohydrate (GO, 95.0%) and glycolic acid (**GC**, 97.0%) were purchased from Wako; N,N-dimethylformamide (99.5%) was purchased from Kanto; Al (99%), Ti (99.5%), V (99.7%), Ni (99%), Zr (99.2%), Nb (99.9%), Mo (99.95%), Cu (99.9%), Sn (99.9%), Pb (99.95%) foils were purchased from Nilaco. All chemicals were used without further purification.

Synthesis of layered protonated titanate

The layered protonated titanates (LPTs) were synthesised according to a previously reported procedure[1]. A mixture of 1 mL of titanium tetrabutoxide, 10 mL of 2-propanol and 30 mL of *N*,*N*-dimethylformamide were transferred into a 50 mL Teflon-lined autoclave and heated in an electric oven at 200 ºC for 20 h. Finally, the product was collected by centrifugation and washed thoroughly with acetone and methanol.

Synthesis of porous TiO_2 spheres

The porous TiO_2 spheres (**PTS**s) were synthesised by calcination of LPTs under flowing air at 150, 300, 450, 500, 525, 550 or 600 ºC for 1 h; the heating rate was 100 ºC/h.

Structural characterization

TEM and HRTEM images were collected on a JEM-2010HCKM (JEOL) operated at 200 kV. An STEM observation and EELS mapping were conducted on a JEM-ARM200F (JEOL) at Kyushu University operated at 200 kV. Sample grids for the TEM, HRTEM, STEM and EELS observations were prepared by dropping ethanol dispersions of the specimens onto a copper grid with no metal coating. XRD measurements were conducted using a SmartLab (Rigaku) with Cu-Kα radiation (λ = 1.54059 Å) at 45 kV and 200 mA. Nitrogen adsorption-desorption measurements were performed at -196 ºC on a BELSORP-max (Bel Japan). The bruner-Emmett-Teller (BET) specific surface areas were calculated from the adsorption data in the relative pressure ranging from 0.04 to 0.2[2]. Pore size distributions were calculated using the isotherms based on the Barrett-Joyner-Halenda (BJH) formula[3]. XPS spectra were recorded on a VersaProbeII (ULVAC-PHI) with Al anode X-ray source. Binding energies were corrected by referring a C 1s binding energy of the carbon atoms of the ligand in the specimens at 284.5 eV. The obtained XPS spectra were reproduced using a combination of Gaussian and Lorentzian functions. UV-vis spectra were recorded on a V-670 spectrometer (JASCO). The diffuse reflection spectra were converted into reflectance spectra using the Kubelka-Munk function.

Preparation of electrodes of a variety of metal and metal oxide electrodes

Al, Ti, V, Ni, Zr, Nb and Mo foils (2×2 cm) were used after calcination at 450 ºC for 0.5 h under air flow. Cu, Sn and Pb foils (2×2 cm) and a Pt coil (23 cm) were used without calcination.

Preparation of TiO_2 catalyst loading Ti foil electrodes

Suspensions of TiO_2 catalyst (10 or 20 mg) in methanol (0.2 mL) were applied to Ti foils (2 × 2 cm^2) previously processed at 450 ºC for 0.5 h. The TiO_2-catalyst-mounted Ti foils were calcined at 150, 300, 450, 500, 525, 550 and 600 ºC under flowing air.

Electrochemical measurements

All electrochemical experiments were conducted using a three-electrode system connected to a VersaSTAT4 potentiostat (AMETEC, Princeton Applied Research). A coiled Pt wire (230 × 0.5 mm^2, BAS) was used as a counter electrode. An Ag/AgCl (RE-1B, BAS) or an Hg/HgO (RE-6A, BAS) reference electrode was used in acidic or alkaline conditions, respectively. Potentials applied to the working electrode were measured against a reference electrode and converted to the RHE reference scale using:

$$E \text{ (versus RHE)} = E \text{ (versus Ag/AgCl)} + 0.199 \text{ V} + 0.059 \text{ V} \times \text{pH}$$

$$E \text{ (versus RHE)} = E \text{ (versus Hg/HgO)} + 0.110 \text{ V} + 0.059 \text{ V} \times \text{pH}$$

OX electrochemical reduction at a constant potential (chronoamperometry, CA) and product analysis

The electrochemical reduction of **OX** at a constant potential, i.e., chronoamperometry (CA), was performed in a two-compartment electrochemical cell sealed with Teflon caps to be gas-tight. A piece of proton-conducting membrane (Nafion®, NRE-212, Sigma-Aldrich) was used as a separator. An aqueous electrolyte solution (40 mL of 0.16 or 0.03 M **OX** and 0.16 or 0.20 M Na_2SO_4) was introduced into a cathodic cell (75 mL in volume), and working, reference, and counter electrodes were placed inside the cell. The pH value of the electrolyte solution (40 mL of 0.16 or 0.20 M Na_2SO_4) in the anodic cell was adjusted by the addition of H_2SO_4 to be identical to that of the electrolyte solution in the cathodic cell. After the Teflon caps were tightly closed, Ar gas was bubbled into both the cathodic and anodic cells for 30 min to purge the air from the cells. **OX** electrochemical reductions were conducted by controlling the working electrode potential using a VersaSTAT4 potentiostat. The reaction solution (50 μL) was collected from the cathodic cell and analysed using a high-performance liquid chromatograph (HPLC, LC-20AD, Shimadzu) equipped with a refractive-index detector (RID-10A, Shimadzu) and a diode-array detector (SPD-M20A, Shimadzu).

GC electrochemical oxidation and product analysis

An ethylene glycol (0.9 g) suspension of 20 wt.% Pt/C (50.5 mg, Wako) was applied onto carbon felts (4 cm^2 × 4 felts, 16 cm^2 total). The loaded felts were heat-treated under N_2 gas at 400 ºC for 30 min and then under H_2 gas at 300 ºC for 10 min. Electrooxidation reactions were performed in a two-compartment electrochemical cell sealed to be gas-tight with Teflon caps. A piece of proton-conducting membrane was used as a separator. Aqueous electrolyte solution (50 mL of 20 wt.% KOH, 0.5 M **GC**) was introduced into an anodic cell (75 mL in volume) into which the working and reference electrodes (Hg/HgO) were subsequently immersed. A counter electrode was placed in a cathodic cell (75 mL in volume) containing aqueous electrolyte solution (50 mL, 20 wt.% KOH). After the Teflon caps were tightly closed, N_2 gas was bubbled in both the anodic and cathodic cells for 30 min to purge the air from the cell. **GC** electrooxidation was conducted at 1.2 V and 50 ºC for 2 h, where the potential was controlled using a VersaSTAT4 potentiostat. The chemical composition of the reaction solution (50 μL) collected from the cathodic cell was analysed using HPLC.

Definition of Faraday efficiency

The Faraday efficiency in the electroreduction experiments is defined by the following equation:

$$Faraday\ efficiency\ (\%) = \frac{m_{products} \times n \times F}{Q} \times 100,$$

where $m_{products}$ is the moles of reduction products; n represents the number of electrons required for the formation of GO and **GC** from **OX** (n = 2 and 4 for the formation of GO and **GC**, respectively) or **OX** from **GC** (n = 4 for formation of **OX**); F is Faraday's constant (96,485 C/mol of electrons); and Q is the total charge in Coulombs passed across the electrode during the electrolysis.

Cyclic voltammetry (CV) measurements

CV measurements were conducted by employing a three-electrode system connected to a VersaSTAT4 potentiostat. An electrolyte aqueous solution (80 mL of 0.03 M **OX** and 0.20 M Na_2SO_4) was introduced into a glass cell (100 mL in volume, ALS). After the glass cell was tightly sealed with Teflon cap, Ar gas was bubbled for 30 min in order to purge the air from the inside of the cell. The current value was recorded against the applied potential with 10 mV/s scan rate and 5 scan cycles. The CV measurement for a blank solution was carried out by following the same procedures abovementioned except for using electrolyte solution (80 mL of 0.20 M Na_2SO_4).

Alkaline fuel cell (AFC) tests

A direct glycolic acid AFC was fabricated using pelletised $LaSr_3Fe_3O_{10}$ powder as an electrolyte. The $LaSr_3Fe_3O_{10}$ powder was synthesised by a solid-state reaction using a procedure previously reported in the literature[4]. A pressed and pelletised $LaSr_3Fe_3O_{10}$ disc (20 mm in diameter and 1 mm in thickness) was pretreated and used as an electrolyte. For the preparation of an anodic electrode, an ethylene glycol (EG) paste containing $LaSr_3Fe_3O_{10}$ and a commercial Pt catalyst (TEC10E40E, Tanaka) was shaped into a 5 mm diameter disk. The anodic and cathodic electrodes were exposed to an aqueous solution (2 M **GC**, 4 M KOH) at 70 ºC and under flowing, wet O_2 flow. Electromotive force and electron density were recorded at a scan rate of 11 mA/s using a potentiostat (Autolab, Metrohm) connected to the cell fixtures.

OX adsorption tests

OX adsorption experiments were performed by suspending 10 mg **PTS**-500 or **PTS**-600 in 5 mL of aqueous solution containing 22.2 mmol **OX** at 24 ºC for 2 h. After the adsorption, **PTS**s were removed from the suspension by centrifugation at 6000 rpm for 3 min. The amounts of **OX** adsorbed on **PTS**s were determined by the HPLC analysis for the supernatant solution.

Energy efficiency calculation

Energy efficiencies (η) for the **OX** electroreduction and **GC** electrooxidation on a working electrode were calculated by the following equation:

$$\eta = \frac{V_t - |V_E|}{V_t} \times \eta_F ,$$

where V_t is a theoretical open-circuit potential using **GC** as a fuel, i.e., 1.1 V, V_E is an applied potential on the working electrodes, i.e., -0.6 V vs. RHE for **OX** electroreduction and 0.6 V vs. RHE for **GC** electrooxidation, and η_F is Faraday efficiency, i.e., 85% for **OX** electroreduction at -0.6 V vs. RHE and 84% for **GC** electrooxidation at 0.6 V vs. RHE.

1 H. B. Wu, X. W. D. Lou, H. H. Hng, *Chem. Eur. J.*, 2012, **18**, 2094.
2 S. Brunauer, P. H. Emmett, E. Teller, *J. Am. Chem. Soc.*, 1938, **60**, 309.
3 E. P. Barrett, L. G. Joyner, P. P. Halenda, *J. Am. Chem. Soc.*, 1951, **73**, 373.
4 T. Takeguchi, T. Yamanaka, H. Takahashi, H. Watanabe, T. Kuroki, H. Nakanishi, Y. Orikasa, Y. Uchimoto, H. Takano, N. Ohguri, *J. Am. Chem. Soc.*, 2013, **135**, 11125.

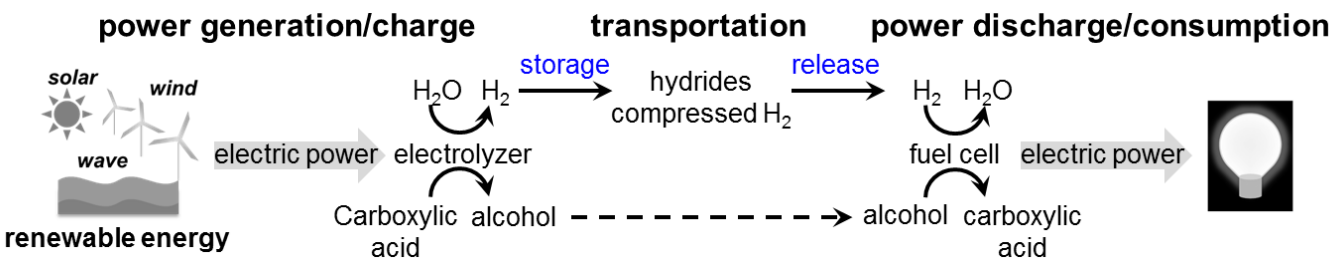

Scheme S1 Comparison between hydrogen and carboxylic acid (R-COOH)/alcohol (R-OH) redox couples as energy carriers.

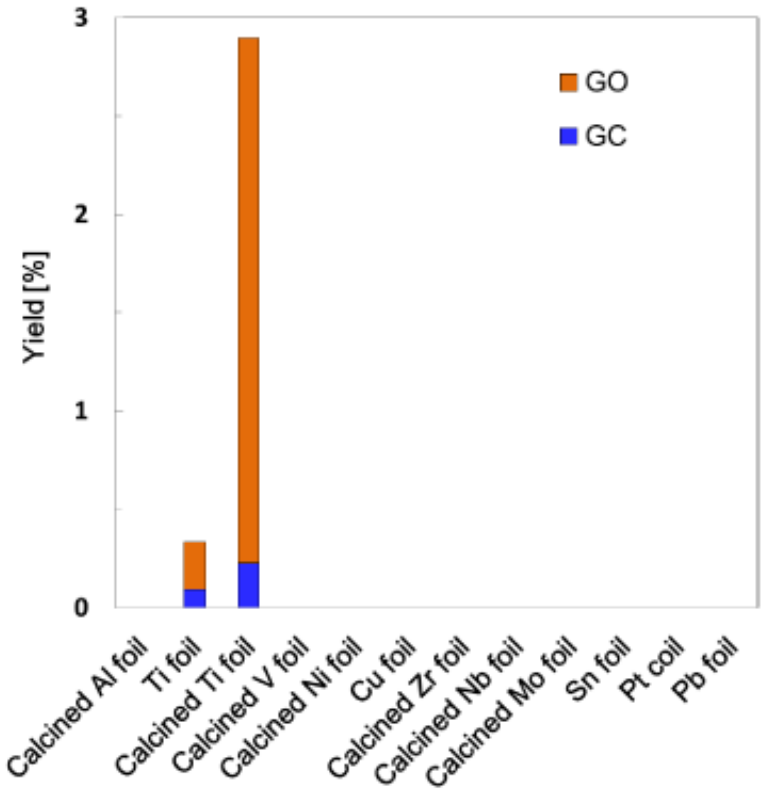

Fig. S1 Product yields on Al, Ti, V, Ni, Cu, Zr, Nb, Mo, Sn, Pt and Pb in **OX** reductions. Al, Ti, V, Ni, Cu, Zr, Nb, Mo, Sn and Pb foils and a Pt coil were used as electrodes for **OX** electroreduction. Al, Ti, V, Ni, Zr, Nb and Mo foils were calcined at 450 ºC. Electroreductions were performed in 0.16 M **OX** with 0.16 M Na_2SO_4 (pH 1.2) at -0.627 V vs. RHE at 24 ºC for 2 h. Orange and blue bars represent **GC** and GO yields, respectively.

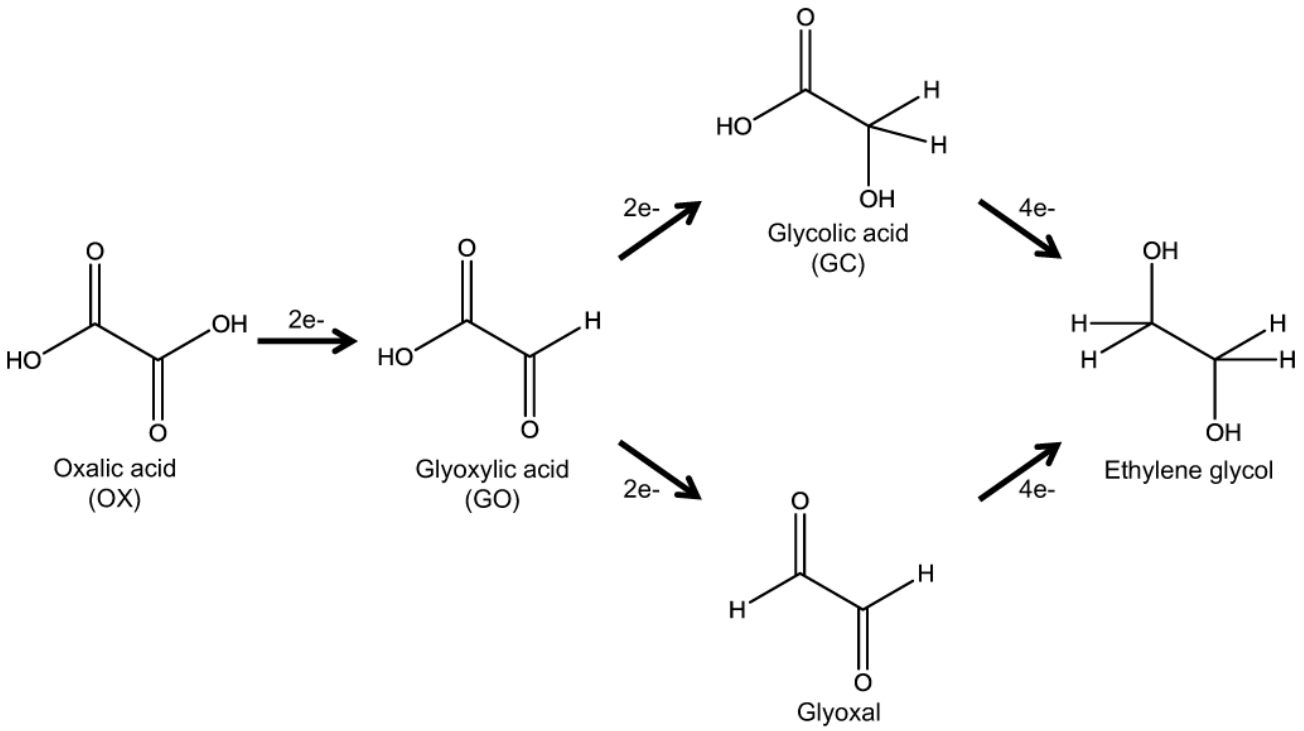

Scheme S2 Compounds possibly produced in the multistep reduction of **OX**.

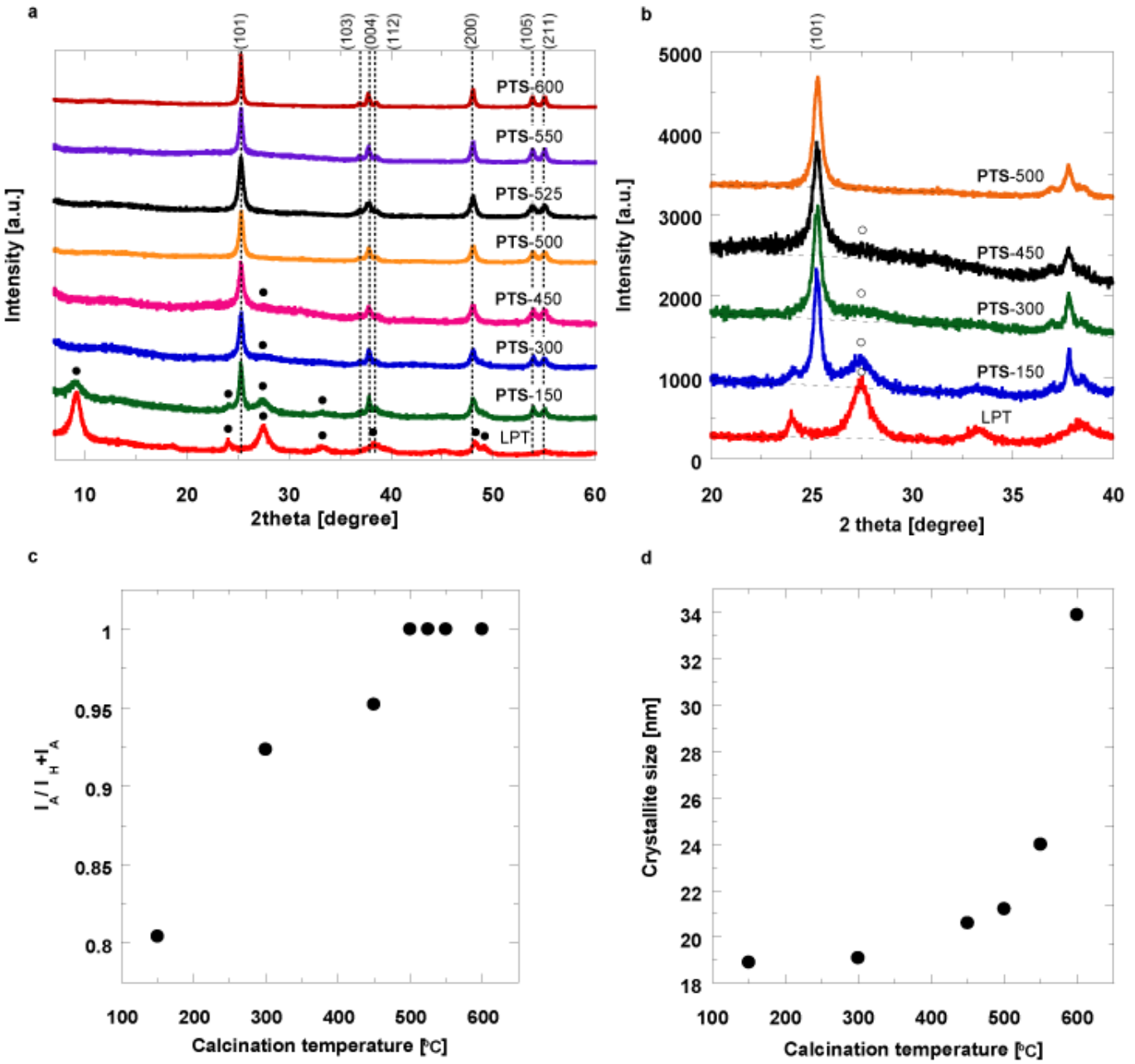

Fig. S2 XRD patterns and structural properties of LPT and **PTS**s. (a) XRD patterns. Broken lines indicate diffraction angles of an anatase-type TiO_2 (JCPDF card file 01-0562). Diffraction peaks assignable to $H_2Ti_2O_5 \cdot H_2O$ are marked with solid circles. (b) Enlarged XRD patterns in the range from 20 to 40°. The solid line indicates the diffraction angle from the (101) plane in anatase-type TiO_2. The diffraction peaks from the (310) plane in $H_2Ti_2O_5 \cdot H_2O$ are marked with open circles. Baselines in the angle range from 20 to 32° are shown as broken lines. (c) I_A/I_H+I_A vs. the calcination temperature, where I_A and I_H indicate the peak intensity from the (101) plane in anatase-type TiO_2 at 2θ = 25.3° and that from the (310) plane in the $H_2Ti_2O_5 \cdot H_2O$ phase at 2θ = 27.4°, respectively. The I_A/I_A+I_H values were calculated to evaluate the extent of anatase phase formation. The I_A/I_A+I_H values increased with increasing calcination temperature up to 500 ºC and became 1 at 500 ºC, implying that **PTS**-500 is composed purely of the anatase phase. (d) The sizes of the crystallites formed in LTS and **PTS**s, as determined by Rietveld profile analysis of their XRD patterns. The calcination temperature dependence reveals that the crystallite sizes of the anatase-type TiO_2 domains progressively increase with increasing calcination temperature.

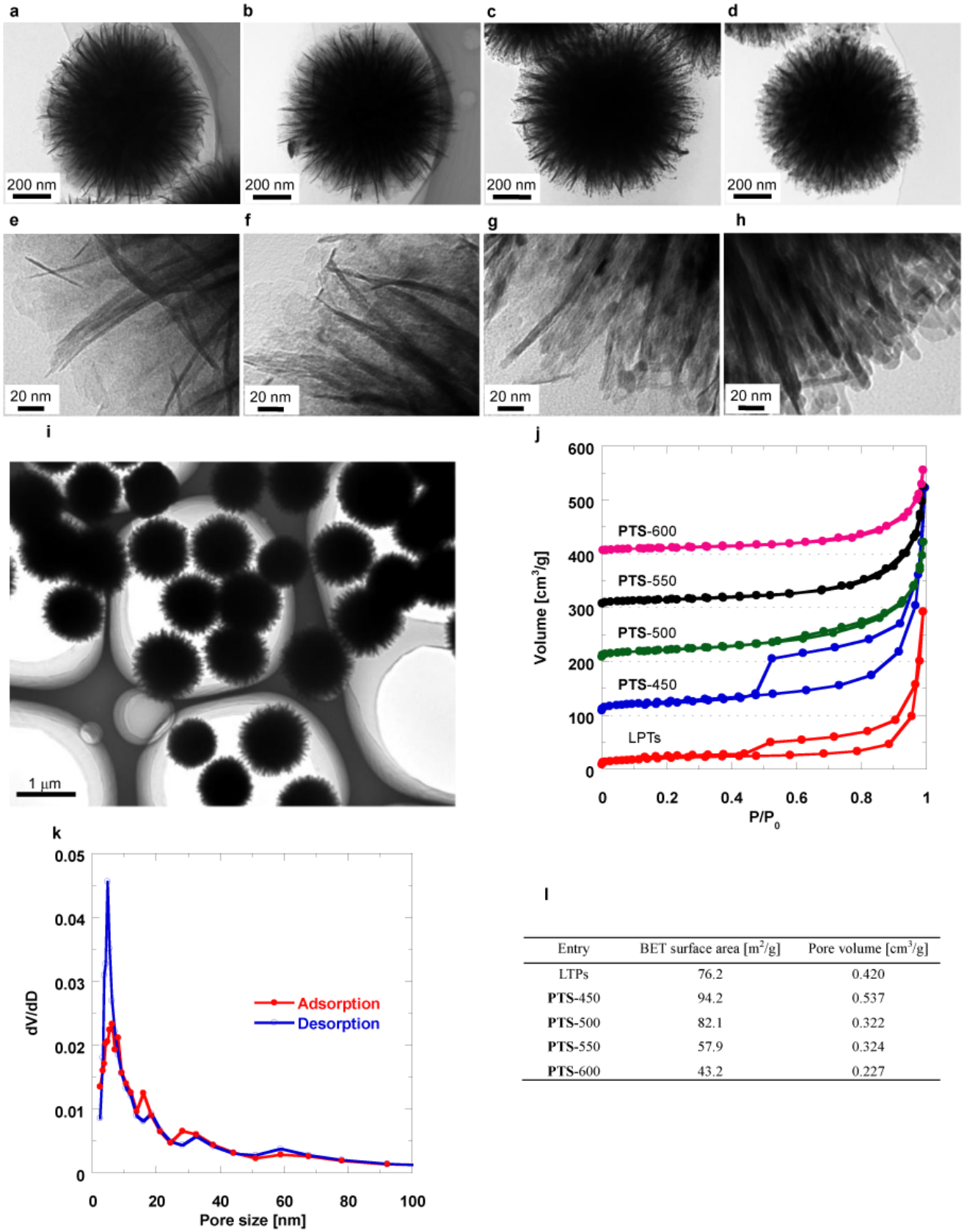

Entry	BET surface area [m^2/g]	Pore volume [cm^3/g]
LTPs	76.2	0.420
PTS-450	94.2	0.537
PTS-500	82.1	0.322
PTS-550	57.9	0.324
PTS-600	43.2	0.227

Fig. S3 TEM images, N_2 absorption isotherms and surface properties of LPT and **PTS**s. Low-magnification (upper) and high-magnification TEM images (lower) of **PTS**-300 (a and e), **PTS**-450 (b and f), **PTS**-525 (c and g), and **PTS**-550 (d and h). (i) Low-magnification TEM image of LPT. (j) Nitrogen adsorption-desorption isotherms of LTP and **PTS**s. All of the N_2 adsorption-desorption isotherms are classified as type IV absorption curves. Type H3 hysteresis loops were observed in the isotherms of LPT and **PTS**-450, suggesting that LPT and **PTS**-450 have slit pores arising from aggregation of the thin nanosheets. Unlike such pore structures, **PTS**-500, **PTS**-550 and **PTS**-600 have straight pores between the nanorods according to their isotherms without hysteresis loops. (k) BJH pore size distributions of **PTS**-500. The pore size distribution shows that the **PTS**-500 has mesopores less than 50 nm in diameter. (l) Table showing a summary of the structural properties of LPT and **PTS**s. Porous structures of **PTS**s lead to high BET surface areas and to large total pore volumes. The relatively small surface area calculated for **PTS**-600 is possibly attributed to the partially aggregated nanostructure, which was observed in TEM and XRD measurements.

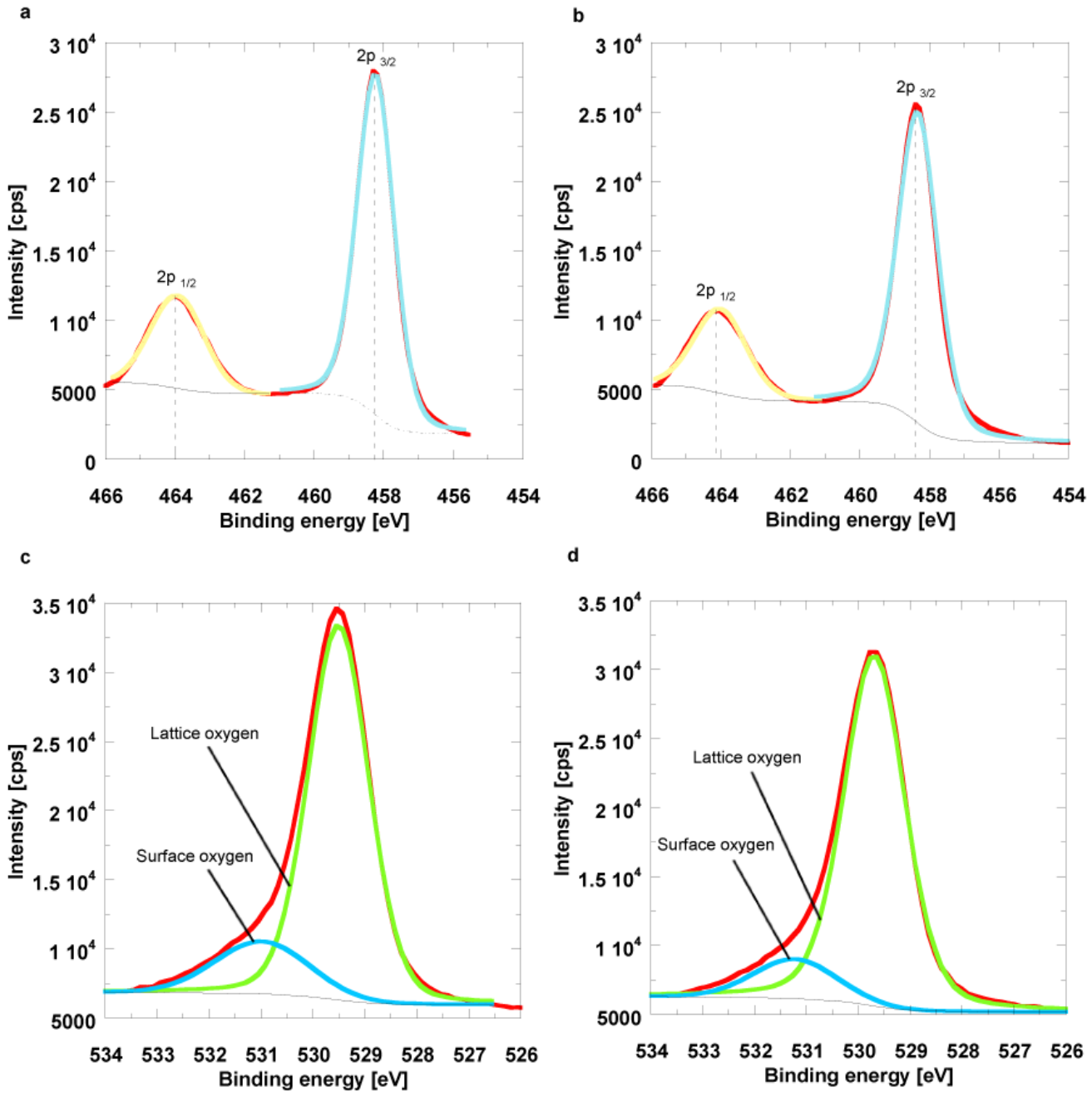

e

	BET surface area [m^2/g]	Adsorbed **OX** [μmol]	Number of adsorbed **OX** per unit area [/10 nm^2]
PTS-500	82.1	1.28	9.4
PTS-600	43.2	0.70	9.7

Fig. S4 Surface properties of **PTS**s. (a) and (b) Ti 2p XPS spectra of **PTS**-500 and **PTS**-600, respectively. Sharp and intense Ti 2p peaks were clearly observed in the spectra of both **PTS**s, and the area ratios of the Ti 2p3/2 and Ti 2p1/2 peaks for **PTS**-500 and **PTS**-600 are almost identical, i.e., 0.360 and 0.340, respectively. These observations indicate that both **PTS**s consist only of Ti^{4+} surface species. (c) and (d) O 1s XPS spectra of **PTS**-500 and **PTS**-600. (e) Table summarising **OX** adsorption properties of **PTS**-500 and **PTS**-600. **OX** adsorption experiments were conducted by suspending 10 mg of **PTS**s in 5 mL of aqueous solution containing 22.2 mmol of **OX** at 24 ºC for 2 h. The amounts of **OX** adsorbed onto the **PTS**s were determined by HPLC analyses.

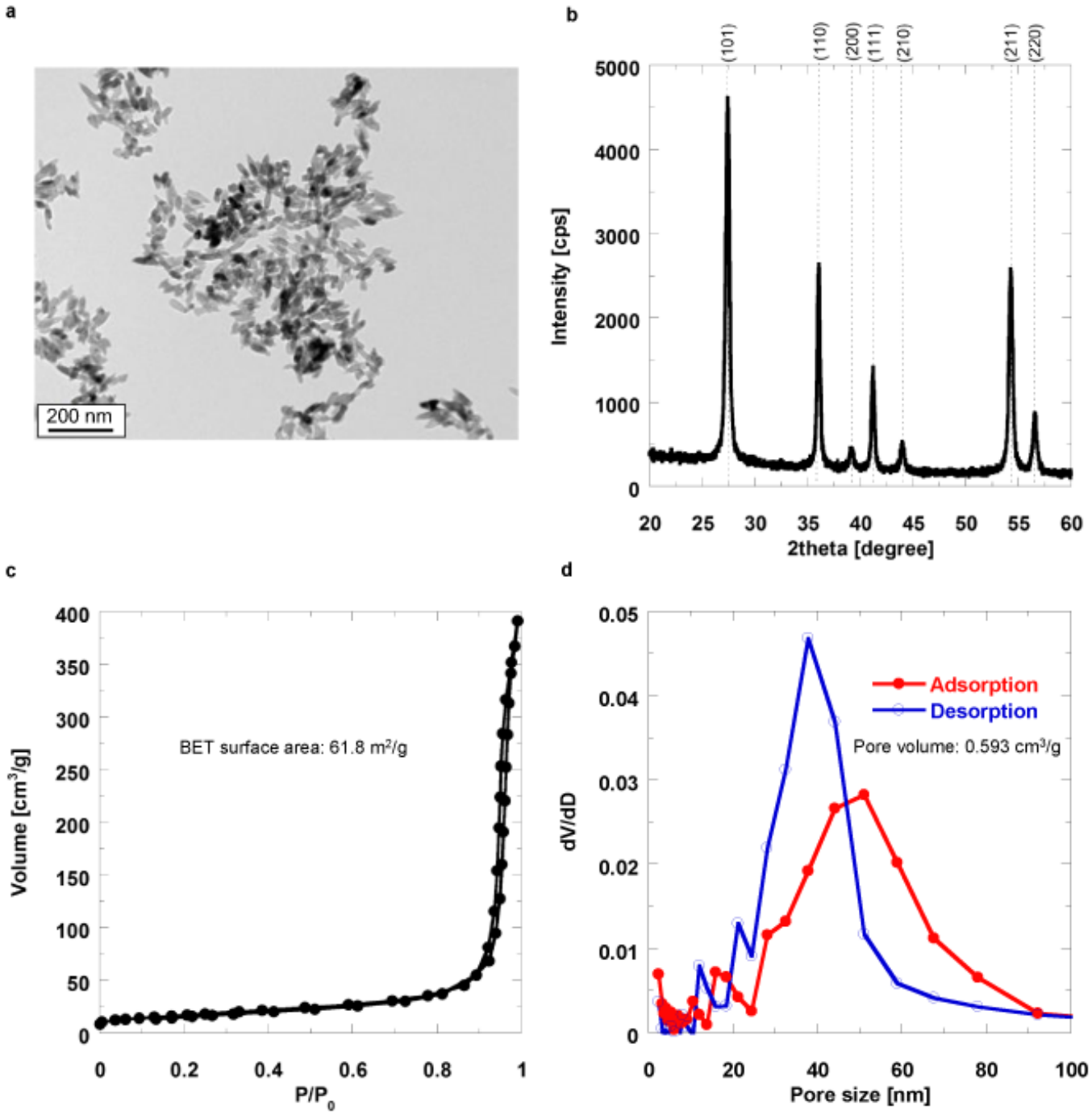

Fig. S5 Structural and surface properties of rutile-type TiO_2 NPs. (a) TEM image, (b) XRD pattern (c) nitrogen adsorption-desorption isotherm, and (d) BJH pore size distributions of rutile-type TiO_2 NPs. Broken lines shown in (b) indicate diffraction angles of rutile-type TiO_2 (JCPDF card file 01-1292).

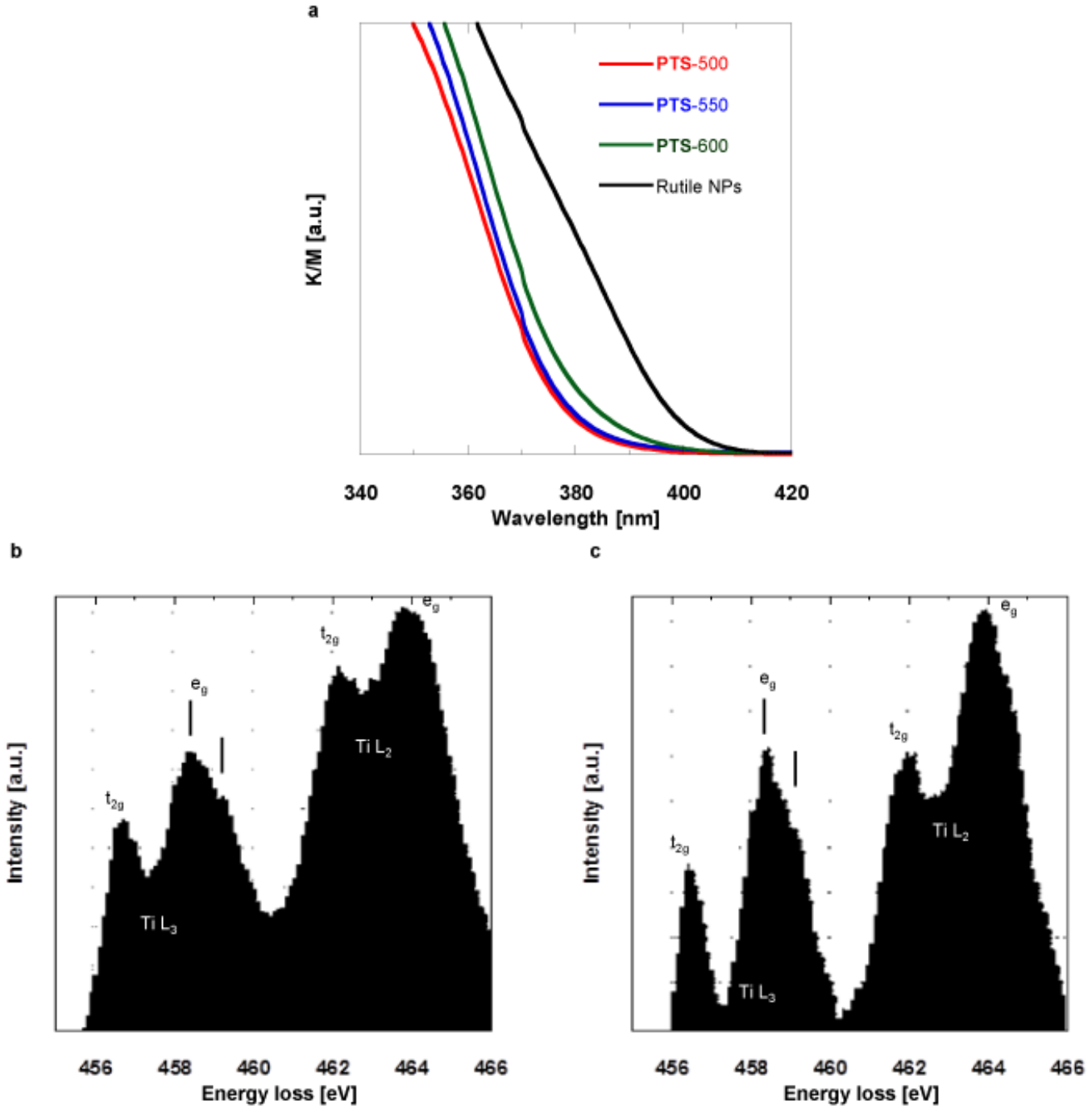

Fig. S6 UV-vis and EELS spectra of **PTS**s. (a) UV-vis spectra of **PTS**-500, **PTS**-550, **PTS**-600 and rutile NPs. (b) and (c) EELS spectra of anatase- and rutile-type TiO_2 phases. Ti L_3 e_g absorption spectra show asymmetric structures, i.e., a shoulder emerging on the high-energy-loss side in anatase and on the low-energy-loss side in rutile.

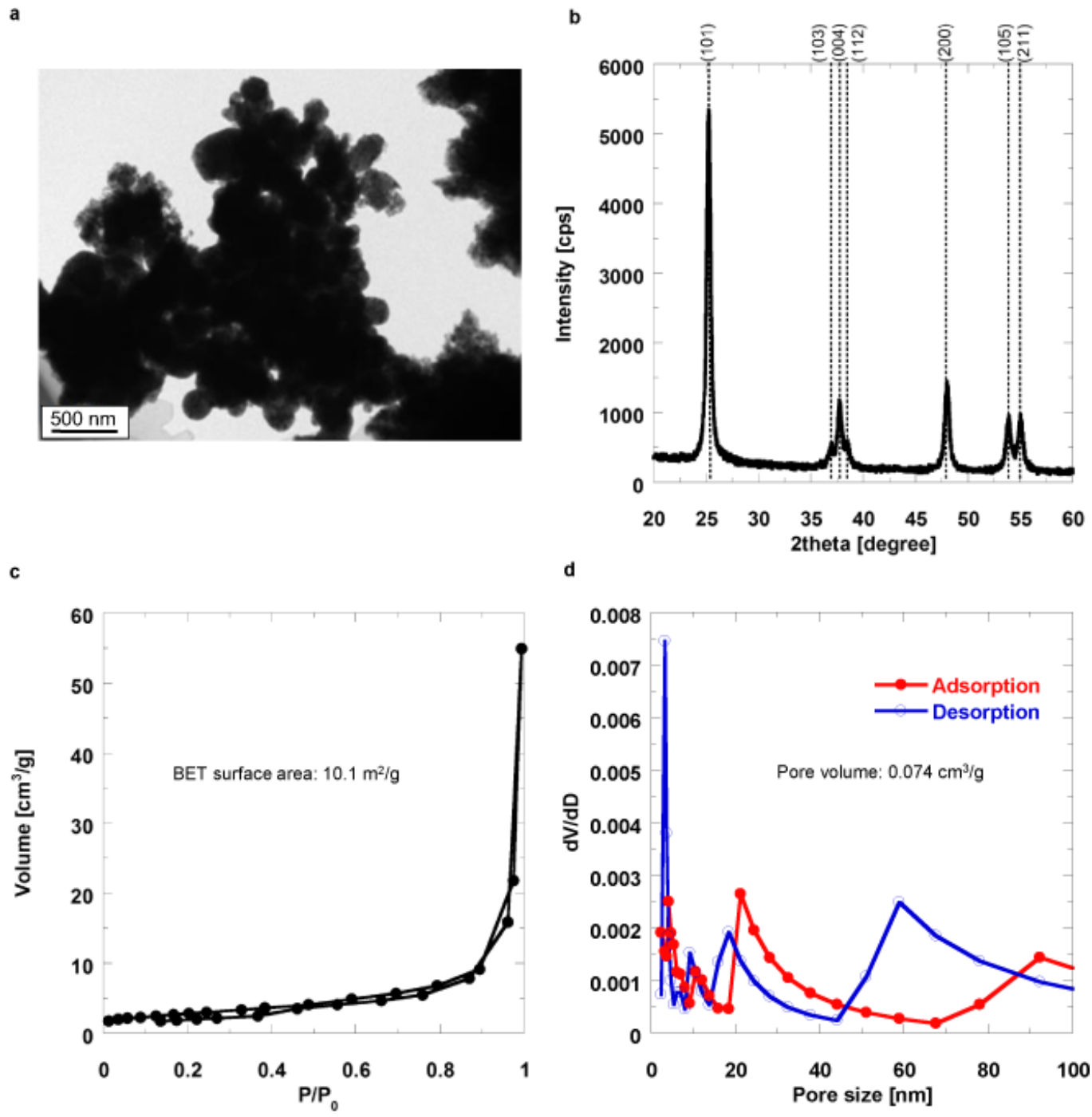

Fig. S7 Structural and surface properties of bulk anatase. (a) TEM image, (b) XRD pattern (c) nitrogen adsorption-desorption isotherm, and (d) BJH pore size distributions of bulk anatase-type TiO_2. Broken lines shown in (b) indicate diffraction angles of an anatase-type TiO_2 (JCPDF card file 01-0562).

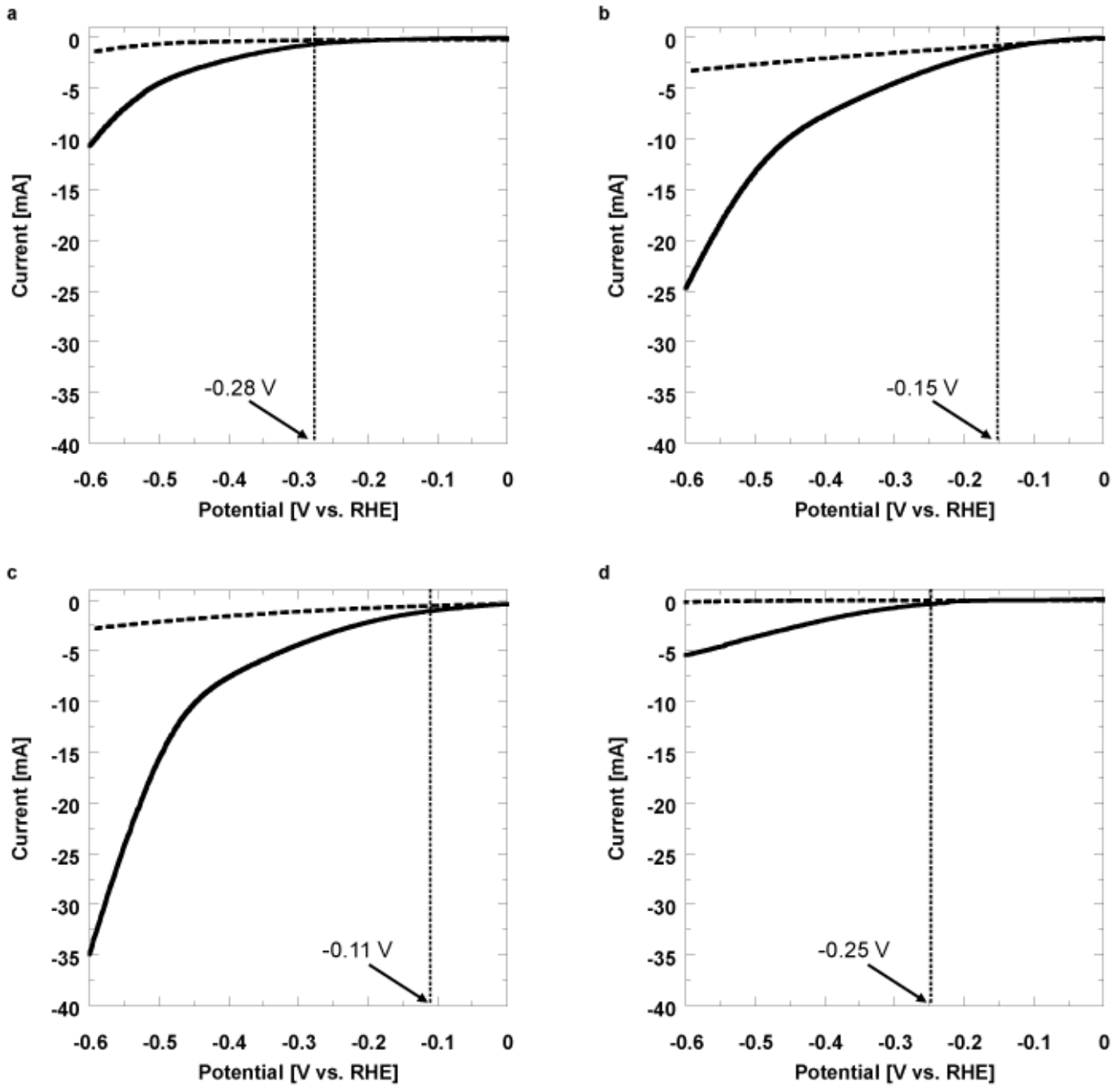

Fig. S8 CV curves for the electroreduction of **OX** using (a) Ti foil and (b) Ti foil modified with **PTS**-450, (c) **PTS**-500 and (d) **PTS**-600. Solid and broken curves represent reduction currents measured in electrolyte solutions with and without the **OX** substrate, respectively. The electrochemical experiments were conducted in 0.03 M **OX** aqueous solution including 0.2 M Na_2SO_4 or 0.2 M Na_2SO_4 (pH 2.1) aqueous solution at 24 ºC.

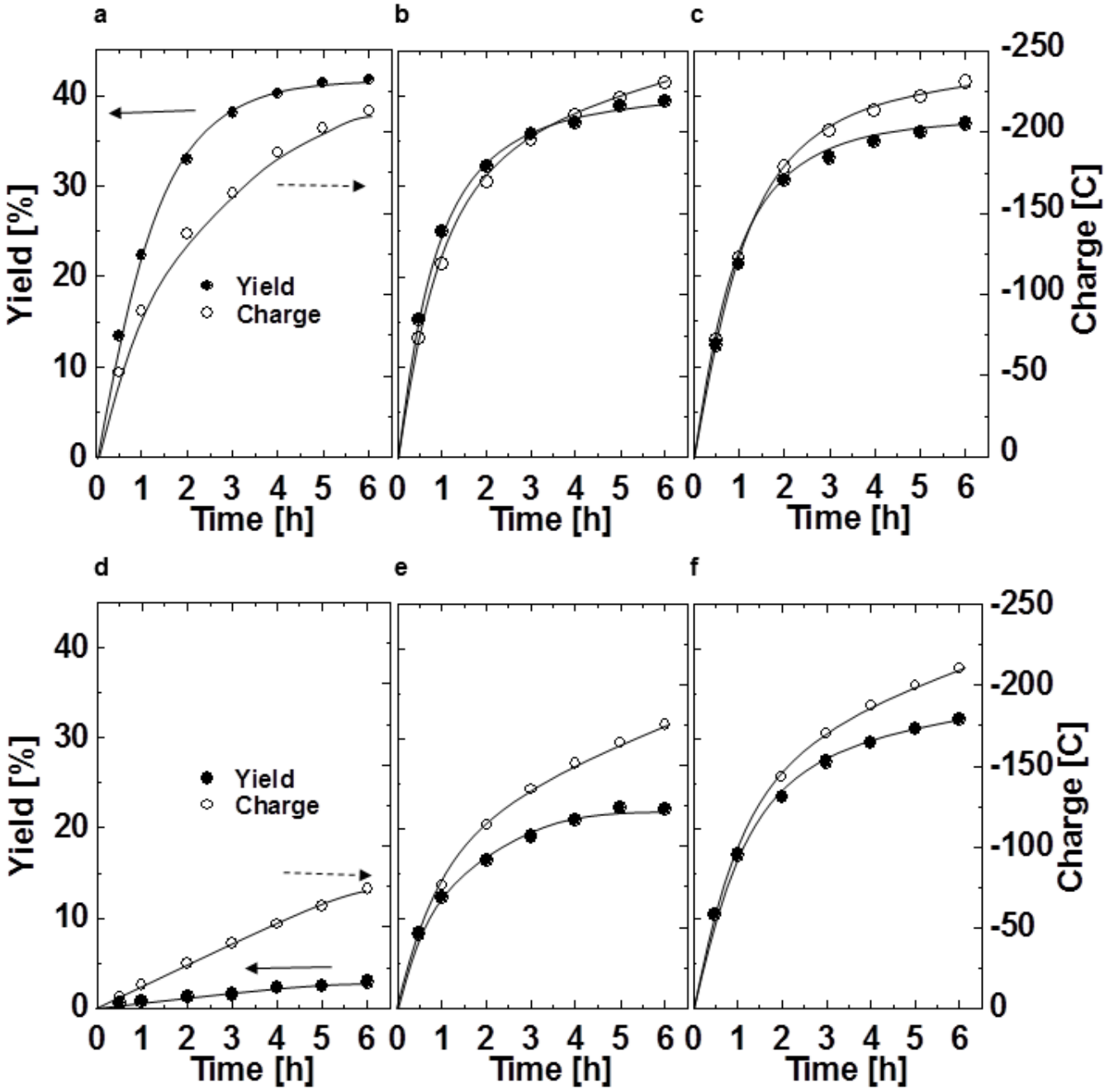

Fig. S9 Additional catalytic performances of **PTS**-500 at various potentials. Total yields (or total charges) for formation of reduction products examined at -0.7 V vs. RHE and various temperatures (top row) and at various potentials and 50 ºC (bottom row). (a) Electrolysis at -0.7 V and 24 ºC. (b) Electrolysis at -0.7 V and 40 ºC. (c) Electrolysis at -0.7 V and 50 ºC. (d) Electrolysis at -0.4 V and 50 ºC. (e) Electrolysis at -0.5 V and 50 ºC. (f) Electrolysis at -0.6 V and 50 ºC. **GC** was obtained with 99% selectivity via electrolysis at 50 ºC for 6 h. All electrochemical experiments, except for the blank measurement, were conducted in 0.03 M **OX** aqueous solution containing 0.2 M Na_2SO_4 (pH 2.1).

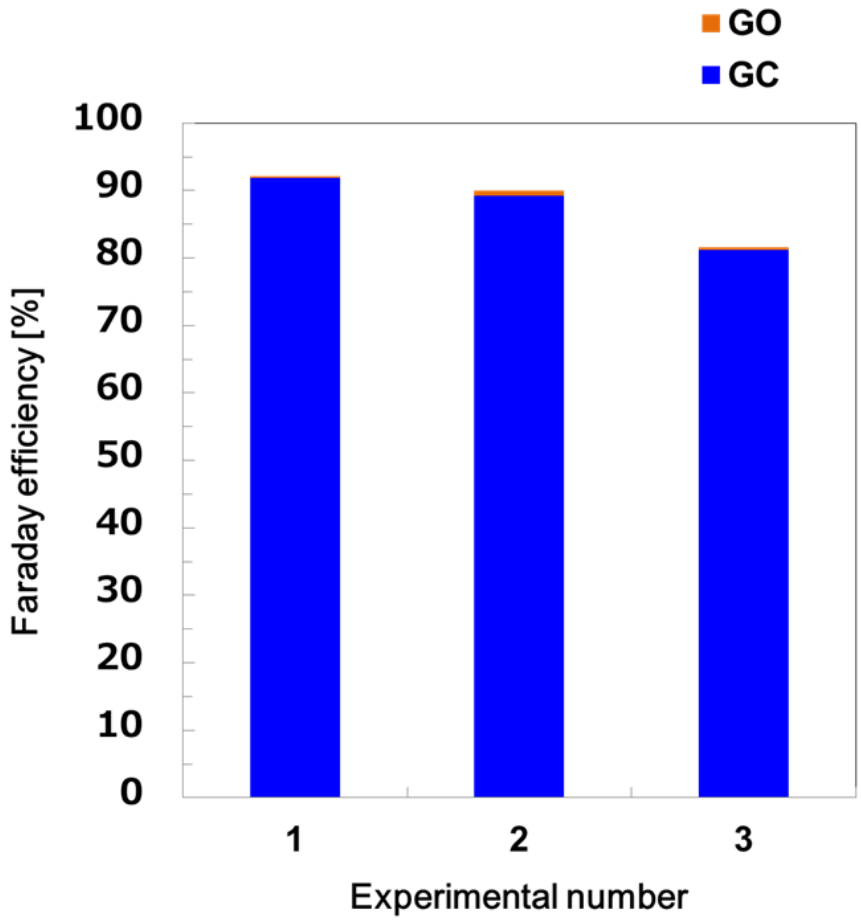

Fig. S10 Faraday efficiencies for a product generation in 3 successive CA experiments for **OX** electroreduction using **PTS**-500. Each **OX** electroreduction was conducted in 0.03 M **OX** aqueous solution containing 0.2 M Na_2SO_4 (pH 2.1) at -0.7 V vs. RHE and 50 ºC for 6 h. Orange and blue bars represent Faraday efficiencies for **GC** and GO generations, respectively.